where

$$C = A[h\nu \ln (R)]^2/\{4e[\alpha_0 L - \ln (R)]^3\} \tag{5}$$

Here we derive a correction to allow for spontaneous emission by including the change of hysteresis loop width δI (see Fig. 2) in terms of the power P_{up} at the switch-up point. The method is to perform a small-signal expansion of eqns. 1–3 around the switch-up current I_{th} in the absence of spontaneous emission, i.e. we assume $(I_{th} - 1) \ll I_{th}$, with corresponding carrier concentrations n_1, n_2 such that $(n_{1th} - n_1) \ll n_{1th}$ and $n_2 \ll N_2$.

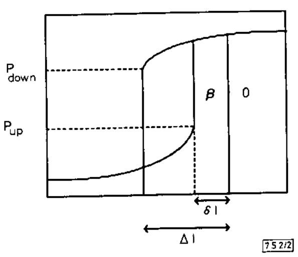

Fig. 2 *Schematic hysteresis loops for zero and nonzero spontaneous emission coefficients, indicating notation used in analysis*

Under these assumptions, eqns. 1–3 yield

$$(I - I_{th})\tau_1\sigma_1/(eV) + x_2\sigma_2^2 N_2 \tau_2 S + x_1\beta_1 n_{1th}/(\tau_1 S) = 0 \tag{6}$$

The value of δI is then given by $(I - I_{th})$ at the extremum, i.e. $dI/dS = 0$. Evaluating this condition in terms of P_{up}, we arrive at an approximation for the corrected form of eqn. 4, namely

$$\sigma_2\tau_2 = [\Delta I - \delta I][P_{down}^2/C - P_{up}/B]^{-1} \tag{7}$$

where

$$B = h\nu\sigma_1\tau_1\{4e\sigma_2 N_2 L x_2[1 - \alpha_0 L/\ln (R)]\}^{-1} \tag{8}$$

We may test the accuracy of this approximation by using the data of Fig. 1. The parameter values used are given in the Figure caption, and when these are used in eqns. 5 and 8 we find $C = 1{\cdot}22 \times 10^{-29}\,\mathrm{mW^2\,cm^2\,s\,mA^{-1}}$ and $B = 4{\cdot}22 \times 10^{-27}\,\mathrm{mW\,cm^2\,s\,mA^{-1}}$. From Fig. 1 we have that $\Delta I = 4{\cdot}5\,\mathrm{mA}$ and $P_{down} = 0{\cdot}3\,\mathrm{mW}$. For $\beta_1 = 10^{-5}$, the approximation used here is quite accurate, because the values of $\delta I = 0{\cdot}8\,\mathrm{mA}$ and $P_{up} = 6\,\mu\mathrm{W}$ from the calculation of Fig. 1 yield a value of $\sigma_2\tau_2 = 5{\cdot}6 \times 10^{25}\,\mathrm{cm^2\,s}$ when used in eqn. 7 (c.f. the true value of $6{\cdot}0 \times 10^{25}\,\mathrm{cm^2\,s}$). For $\beta_1 = 10^{-4}$, the approximation is rather worse, because the corresponding values are $\delta I = 2{\cdot}2\,\mathrm{mA}$, $P_{up} = 20\,\mu\mathrm{W}$ and $\sigma_2\tau_2 = 4{\cdot}6 \times 10^{25}\,\mathrm{cm^2\,s}$. However, more serious concerns about the use of this approximation on experimental data are

(*a*) the difficulty of obtaining good estimates for the quantities appearing in the coefficient B as defined by eqn. 8, especially σ_1, τ_1 and the total saturable absorption $(\sigma_2 N_2)$

(*b*) the problem of determining a sufficiently accurate experimental value for P_{up}.

Conclusion: It has been shown that the spontaneous emission into the lasing mode can strongly affect the width of the hysteresis loop predicted from rate equations for bistable laser diodes with segmented contacts. This effect can lead to errors in the value of differential gain for the absorber deduced from experimental L–I curves. An approximate correction (eqn. 7) to allow for the effect of spontaneous emission has been derived for use in the analysis of experimental data. However, its use in practice would demand extremely accurate measurements of L–I characteristics, together with supplementary measurements of differential gain and lifetime for the amplifying section and the total saturable absorption in the absorber.

Finally, it is worth noting that the inclusion of the spontaneous emission coefficient yields hysteresis loops which closely resemble those measured experimentally [4], particularly with respect to the ratio of upper branch powers at the switch-up and switch-down points. By contrast, when spontaneous emission is neglected this ratio is generally calculated to be far greater than that observed experimentally. This feature therefore adds support to our main conclusion that spontaneous emission into the lasing mode must be included in calculations of L–I characteristics for absorptive bistable laser diodes.

6th January 1992

M. J. Adams, P. E. Barnsley and J. Chen* (*BT Laboratories, Martlesham Heath, Ipswich IP5 7RE, United Kingdom*)

* Present address: Optoelectronics Department, Sichuan University, Chengdu 610064, People's Republic of China

References

1 SUZUKI, S., TERAKADO, T., KOMATSU, K., NAGASHIME, K., SUZUKI, A., and KONDO, M.: 'An experiment on high speed optical time-division switching', *J. Lightwave Technol.*, 1986, **LT-4**, (7), pp. 894–899

2 BARNSLEY, P. E., and FIDDYMENT, P. J.: 'Wavelength conversion from 1·3 to 1·55 μm using split contact optical amplifiers', *IEEE Photonics Technol. Lett.*, 1991, **3**, (3), pp. 256–258

3 BARNSLEY, P. E., and FIDDYMENT, P. J.: 'Clock extraction using saturable absorption in a semiconductor nonlinear optical amplifier', *IEEE Photonics Technol. Lett.*, 1991, **3**, (9), pp. 832–834

4 CHEN, J., BARNSLEY, P. E., and WICKES, H. J.: 'Method of determining differential gain coefficient for bistable laser diodes', *Electron. Lett.*, 1991, **27**, (19), pp. 1745–1747

5 KUZNETSOV, M.: 'Theory of bistability in two-segment diode lasers', *Opt. Lett.*, 1985, **10**, (8), pp. 399–401

6 SUEMATSU, Y., AKIBA, S., and HONG, T.: 'Measurement of spontaneous emission factor of AlGaAs double-heterostructure semiconductor lasers', *IEEE J. Quantum Electron.*, 1977, **QE-13**, (8), pp. 596–600

LOW-VOLTAGE LOW-POWER INFRA-RED RECEIVER FOR HEARING AIDS

A. C. van der Woerd

Indexing terms: Biomedical electronics, Infra-red receivers, Optical receivers, Optoelectronics, Integrated optics

A novel design for an integrated infra-red receiver for remotely controllable hearing aids is presented. Special attention has been paid to insensitivity to DC photocurrents and minimal power consumption. The circuit has been designed for operation at a single supply voltage of 1·0 V.

Introduction: Because of its invisibility to others, most people with moderate hearing loss prefer a hearing aid that is mounted within the ear duct. As the small dimensions of such instruments obstruct the application of hand control, they must be remotely controlled. Three different systems for remote control in hearing aids are presently in use. They use ultrasound, infra-red or radio frequencies as information carriers, respectively. Owing to its immunity to spurious signals and its quick response, infra-red systems, such as have been applied for many years in consumer electronics, should be preferred.

Fig. 1 depicts a block diagram of the complete control system. IR-modulated codewords are received by a photo-

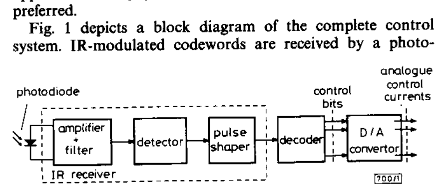

Fig. 1 *Block diagram of complete control system*

diode. Its signals are amplified, filtered, detected and shaped in the IR receiver, whereafter they are decoded into current bits. These are converted into analogue currents controlling volume levels, filter transfers and a standby position by a suitable D/A convertor.

The currently used IR-transmitter circuits can be directly applied to hearing aids, provided that a special set of codes is reserved for that application. However, owing to the special boundary conditions which must be acounted for, the currently used receiver circuits are useless for hearing aids and need to be redesigned. Fig. 2 depicts a block diagram of a traditional infra-red receiver. The light signal, containing digital codewords AM-modulated on a 36 kHz carrier, are picked up by the reverse-biased photodiode D and filtered by an L–C circuit. The most important function of this filter circuit is short circuiting the DC and low-frequency spurious signals caused by sunlight and artificial light sources. The filtered signal is amplified, detected and shaped.

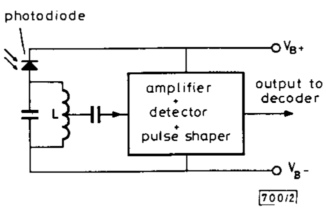

Fig. 2 *Block diagram of traditional IR receiver*

The configuration of Fig. 1 is not suitable for application in (very small) hearing aids for the following reasons:

(*a*) The employed inductor L takes too much space and weight and must, therefore, be avoided.

(*b*) If the instrument is placed in bright sunlight, the photocurrent will discharge the battery.

(*c*) Circuits must be able to operate at a single supply voltage down to 1·0 V (zinc-air cell at end of lifetime.) Currently employed circuits do not meet this requirement.

(*d*) As the receiver must be continually in operation, the power consumption should be kept as low as possible (typically a few tens of microwatts).

General design aspects: The traditionally applied inductor mentioned in the preceding Section (item (*a*)) can be avoided by an active gyrator circuit loaded with a capacitor. Furthermore, the negative effect of the DC photocurrent (item (*b*)) can be fully coped with by biasing the photodiode with a small forward voltage (about 200 mV). A careful design of the circuit architecture can make the circuit suitable for a very low supply voltage (item (*c*)). The demand for minimal power consumption (item (*d*)), however, means a serious restriction on the maximum dynamic range of the system, because noise matching of the first amplifier stage would need an impractically high bias current. This has a negative effect on the obtainable distance range of the transmitter/receiver system. Fortunately, this is not a large problem in applications with hearing aids: a distance range of, say, 1 m is sufficient.

Process choice: Apart from the analogue circuits, the chip must contain a large digital part and a number of D/A convertors for the processing of the received infra-red commands. An I^2L-compatible high-frequency process is chosen for the following reasons:

(1) Available CMOS processes with very low threshold voltages (about or $\pm 0{\cdot}5$ V) are not (yet) sufficiently characterised for analogue applications in the production phase. Analogue CMOS processes with higher threshold voltages are not suitable for the present application, unless a battery voltage multiplier is added to the circuit. This implies that a number of extra discrete capacitors must be added [1]. This is not feasible due to problems of space. CMOS processes must be rejected, therefore, for the time being. Hence, a bipolar process must be chosen.

(2) As a large amount of the chip will be filled with I^2L gates for the digital processing, a realisation of the IR receiver together with all other analogue circuits in an I^2L-compatible low-frequency bipolar standard process would give rise to chip dimensions too large for the present application. Owing to its large component density, the remaining possibility is an I^2L-compatible high-frequency bipolar process.

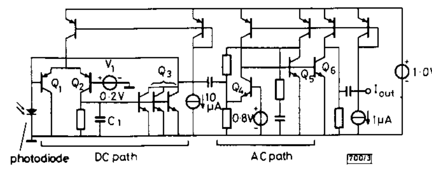

Fig. 3 *Circuit diagram of IR receiver for hearing aids*

Practical circuit: Fig. 3 depicts a (simplified) circuit diagram of a practical IR receiver for hearing aids. The AM detector and the pulse shaper are not included. The photodiode is kept forward-biased by the voltage source V_1. Owing to the very large loop gain of the gyrator circuit ($Q_{1,2,3}$), all practically occurring photocurrents caused by low-frequency spurious signals, DC included, are completely suppressed. The desired signals are amplified by an amplifier with overall feedback ($Q_{4,5}$) and indirect current output (Q_6). The bias currents of $Q_{4,5}$ have been chosen to be 1 μA. At these collector currents the transit frequency of the transistors has decreased in such a way that the high-frequency rolloff of the amplifier is restricted to 36 kHz, so that high-frequency spurious signals also are suppressed. The circuit requires one external component (the capacitor $C_1 = 100$ nF).

To test its feasibility for practical applications, a circuit based on Fig. 3 has been realised in a semicustom process. In the following Section some measurement results are given.

Measurement results: The output signal of the circuit has been measured with the following input signals:

(*a*) a continuous signal with a frequency sweep from 10 Hz to 50 kHz from an IR transmitter; the AC photocurrent amounted to 1 μA (this is a practical value, if the distance between a regular IR transmitter and the receiver is about 1 m)

(*b*) the same input signal with an extra DC light source that causes a DC photocurrent of 500 μA (this value exceeds all practically occurring DC)

(*c*) a practically occurring codeword from an IR transmitter, modulated on a 36 kHz carrier; the distance between transmitter and receiver amounted to 1 m: here the spectrum of the output signal was measured

(*d*) the same signal together with a DC photocurrent of 500 μA.

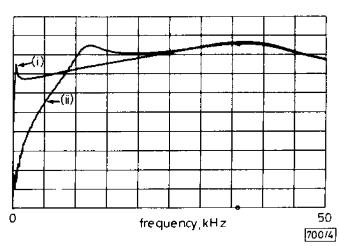

Fig. 4 *Measured transfer function*
(i) without DC photocurrent
(ii) with DC photocurrent

The measurement results are shown in Figs. 4 and 5, respectively. From these results it can be concluded that the extra DC photocurrent hardly affects the transfer function (Fig. 4) and the signal spectrum around a frequency of 36 kHz (Fig. 5).

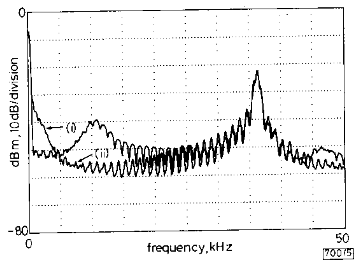

Fig. 5 *Measured output spectrum*
(i) without DC photocurrent
(ii) with DC photocurrent

Finally, the measured total power consumption of the circuit amounted to $24\,\mu W$.

2nd January 1992

A.C. van der Woerd (*Delft University of Technology, Department of Electrical Engineering, Electronics Research Laboratory, Mekelweg 4, 2628 CD Delft, The Netherlands*)

Reference

1 CALLIAS, F., SALCHLI, F. H., and GIRARD, D.: 'A set of four IC's in CMOS technology for a programmable hearing aid', *IEEE J. Solid-State Circuits*, **SSC-24**, (2), pp. 301–312

FAST CALCULATION METHOD FOR MULTICOMPONENT WIGNER-VILLE DISTRIBUTION

W. Pan

Indexing terms: Signal processing, Digital signal processing, Mathematical techniques

Owing to its bilinear nature, calculation of the Wigner-Ville distribution (WVD) produces crossterms between independent frequency components. Usually an averaging technique is adopted to smooth out these terms, the calculation time being proportional to the averaging times. Using the linear nature of averaging and Fourier transform (FT), this technique is improved resulting in a range saving of calculation time.

Crossterms: A typical two-component analytical signal is

$$x(n) = e^{j(n\omega_1 + \phi_1)} + e^{j(n\omega_2 + \phi_2)} \tag{1}$$

The discrete Wigner-Ville distribution (DWVD) using a rectangular window of length $2L + 1$ is [1]

$$\begin{aligned} W_x(n, \omega) &= \text{sind}_L(\omega - \omega_1) + \text{sind}_L(\omega - \omega_2) \\ &\quad + 2\cos[(\omega_1 - \omega_2)n + \phi_1 - \phi_2] \\ &\quad \times \text{sind}_L\left(\omega - \frac{\omega_1 + \omega_2}{2}\right) \end{aligned} \tag{2}$$

where $\text{sind}_L(x) = \sin[(2L + 1)x]/\sin x$.

We see that there is a crossterm between ω_1 and ω_2, of frequency $(\omega_1 + \omega_2)/2$ and modulated with frequency difference signal. When ω_1 and ω_2 are far apart, it is simply an unnecessary interference and is often easily smoothed out by averaging spectra in a period of

$$S = \frac{2\pi}{\omega_1 - \omega_2} \tag{3}$$

When the two components are close, its existence substantially reduces the spectral resolution; the averaging period or the number of DFTs increases in inverse proportion to $\omega_1 - \omega_2$. Therefore a direct averaging technique is practically prohibited of distinguishing close components and the WVD estimator cannot demonstrate its advantage of high frequency resolution.

Reducing the averaging computation: Let us examine WVD formulation from the end. The finite lengthened DWVD is

$$W_x(n, \omega) = \sum_{m=-L}^{L} x(n + m)x^*(n - m)e^{-j2m\omega} \tag{4}$$

or the DFT of kernel $K_n(m) = x(n + m)x^*(n - m)$. Because both the DFT and average are linear transformations, their order is exchangeable. We may average the kernel on n first, then only one DFT is needed to produce the averaged spectrum. The computation time of the set kernel increases with S, but it is far less than calculating an FFT [2] S times before averaging the spectra.

Example: The test analytical signal consists of two components $\omega_1 = 2\pi/8$ and $\omega_2 = 2\pi(1.04/8)$ computed on an IBM 286 computer. To obtain a 512 point DWVD spectrum, the old technique takes 49 min, and the improved takes only 107 s.

13th December 1991

W. Pan (*Digital Signal Processing Division, Department of Radio Engineering, Southeast University, Nanjing 210018, People's Republic of China*)

References

1 VELEZ, E. F., and ABSHER, R. G.: 'Spectral estimation based on the Wigner-Ville distribution', *Signal Process.*, 1990, **20**, (4), pp. 325–346
2 BERGMANN, N.: 'New formulation of discrete Wigner-Ville distribution', *Electron. Lett.*, 1991, **27**, (2), pp. 111–112

GSMBE GROWN (GaIn)P/GaAs HETEROJUNCTION BIPOLAR TRANSISTORS EXHIBITING CURRENT GAINS UP TO 590

S. S. Lu and C. C. Huang

Indexing terms: Bipolar devices, Transistors, Semiconductor devices and materials

The first lattice-matched $Ga_{0.51}In_{0.49}P/GaAs$ heterojunction bipolar transistor grown by gas-source molecular beam epitaxy is reported. Small signal current gains exceeding 590 and small offset voltages (~120 meV) were obtained. These results demonstrate that (GaIn)P is a good alternative to the (AlGa)As in GaAs-based devices.

Introduction: Heterojunction bipolar transistors (HBT) have been shown to be very promising in the area of microwave applications. These devices have been made and studied in several material systems, but most extensively in the GaAlAs/GaAs system. Recently, there has been interest in the $Ga_{0.51}In_{0.49}P/GaAs$ material system because of its larger valence band discontinuity ($\Delta E_v = 0.24$–0.3 eV [1–4], 0.4–0.43 eV [5, 6]) and smaller conduction band discontinuity ($\Delta E_c = 0.19$–0.22 eV [1–4], 0.03–0.06 eV [5, 6]) compared with the band discontinuities of the AlGaAs/GaAs material system for the same bandgap energy difference. The $Ga_{0.51}In_{0.49}P/GaAs$ heterostructure, where most of the